Molecular Motion in Supramolecular Ionic Crystal of Swiss Cheese Structure

Kazuya Kanamaru,[1] Kiyonori Takahashi,[1,2*] Rui-Kang Huang,[1,2] Chen Xue,[1,2] Jia-bing Wu,[1,2] Shin-ichiro Noro[3] and Takayoshi Nakamura[1,2,4*]

[1]Graduate School of Environmental Science, Hokkaido University, N10W5, Kita-ku, Sapporo, Hokkaido, 060-0810
[2]Research Institute for Electronic Science, Hokkaido University, N20W10, Kita-ku, Sapporo, Hokkaido, 010-0020
[3]Faculty of Environmental Earth Science, Hokkaido University, N10W5, Kita-ku, Sapporo, Hokkaido, 060-0810, Japan
[4]Department of Chemistry, Graduate School of Advanced Science and Engineering, Hiroshima University, Higashi-hiroshima 739-8526, Japan

*Corresponding author: Hokkaido University, N10W5, Kita-ku, Sapporo, Hokkaido, 060-0810. Email: ktakahashi@es.hokudai.ac.jp

Abstract

In most molecular crystals, crystal structure collapses when solvent molecules are removed. We report the crystal of (isobutylammonium$^+$)(dibenzo[18]crown-6)[Ni(dmit)$_2$]$^-$•0.4CH_3CN with Swiss cheese-like structure, in which 60% of the CH_3CN sites are voids. The motion of isobutylammonium$^+$ adjacent to the void sites maintains the single crystallinity, which occupy an apparently larger volume than in the static state. This study opens up the possibility of developing novel relaxor dielectrics based on molecular motion in the crystal of partially occupied voids.

Keywords: molecular motion in solid state, crystal engineering, dielectric property

Graphical abstract

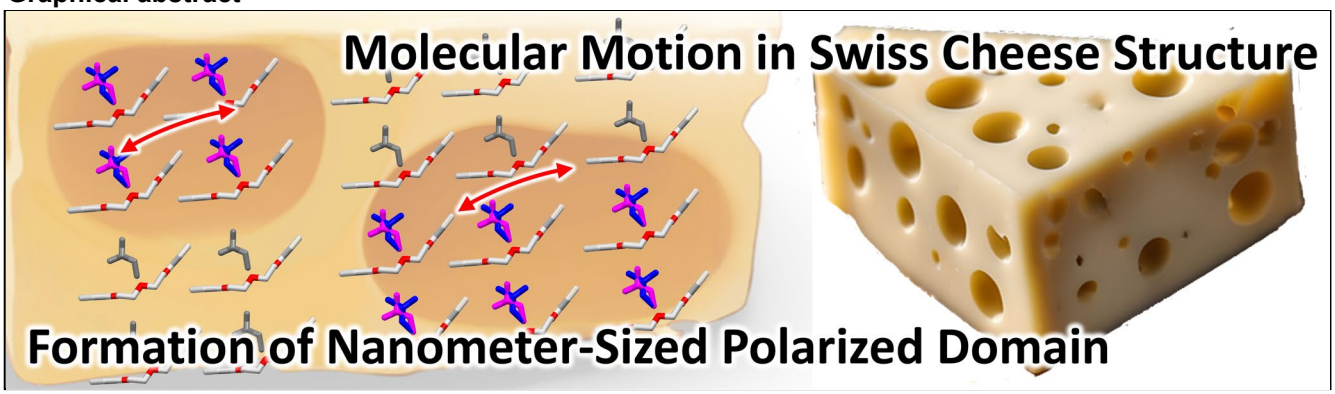

Crystals are usually closely packed and it isn't easy to achieve molecular motion in crystals.[1] If a densely packed structure is difficult to obtain due to the imbalance between the size and shape of the packing molecules, solvent molecules often enter the remaining space and the crystalline structure is maintained.[2–5] As ordinary molecular crystals do not have a strong backbone like metal-organic frameworks, the crystal structure almost always collapses when solvent molecules are removed by heating or other treatments.[6] If the crystalline nature is maintained even after solvent desorption, the space can be used to realize molecular motion within the crystal, opening up the possibility of developing various functionalities originating from molecular motion.

Conversely, the collapse of crystals may be prevented by the dynamic filling of crystal vacancies by molecular motions within the crystals.[7–9] For example, crystals of [Fe^{II}_2(*o*-NTrz)$_5$(NCS)$_4$]•3CH_3OH (*o*-NTrz = 4-(*o*-nitrobenzyl)imino-1,2,4-triazole)) retain their single crystallinity even when three molecules of CH_3OH per composition are removed. In the presence of solvent molecules, all *o*-NTrz ligands are ordered. When the solvent molecules are removed, one $\mu_{1,2}$-bridging ligand located at the center of the C_2 axis is disordered at two equivalent sites and dynamically fills the space.[7] A mixed crystal composed of durene and *p*-dibromobenzene, which has a smaller molecular volume, has the same crystal structure as durene. In the mixed crystal, the crystal structure is maintained by the rotation of *p*-dibromobenzene, which achieves

an average structure of durenes and fills the spaces within the crystal.[10]

We have proposed the supramolecular approach to realize molecular motion in the solid phase and developed variety of electrical and magnetic functions.[11–15] For example, in (*m*-FAni$^+$)(DB18C6)[Ni(dmit)$_2$]$^-$ (*m*-FAni$^+$, DB18C6, and dmit^{2-} are *m*-fluoroanilinium$^+$, dibenzo[18]crown-6, and 1,3-dithiole-2-thione-4,5-dithiolate, respectively), *m*-FAni$^+$ can undergo flip-flop rotational motion in the crystal with the C-N bond as the rotational axis. The dipole moment originating from the *meta*-fluoro group is inverted as the rotation takes place. Since this motion occurs cooperatively in the crystal, the crystal shows ferroelectricity. Here, the phenylene group introduced into DB18C6 secures the rotational space for the *m*-FAni$^+$ based on the C-H•••π interaction between the DB18C6 molecules.[15]

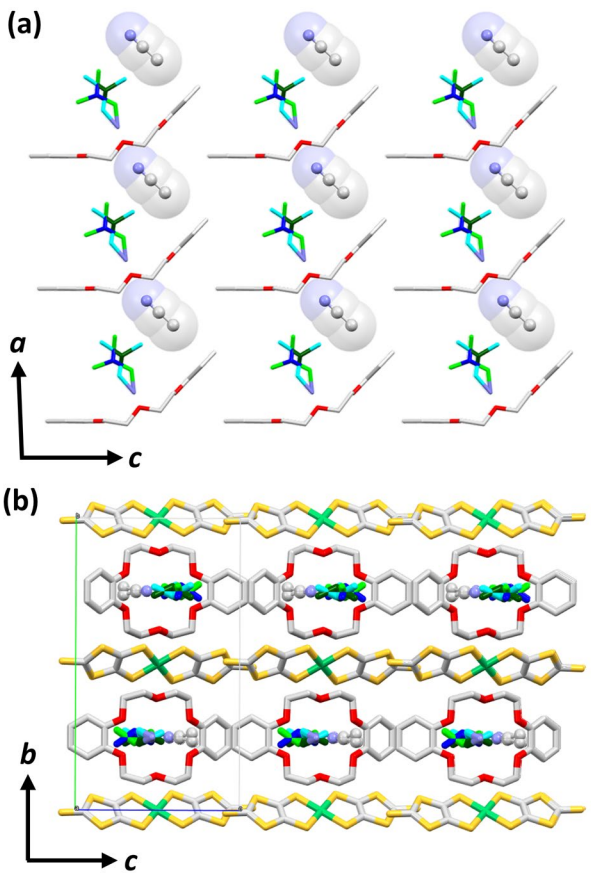

Fig. 1. Packing structure of **1**•0.4CH$_3$CN at 200 K. CH$_3$CN are depicted as ball and stick model and the others are modeled by stick. Carbon, nitrogen, oxygen, sulfur, and nickel are colored by gray, light-blue, red, yellow, and light-green, respectively, except iBA$^+$ cations showing disorder. Hydrogen atoms are omitted for clarity. (a) Supramolecular cation layer viewed along the *b* axis. (b) Packing structure viewed along the *a* axis.

In crystals where molecular motion spatially occupies solvent-free defect sites and keeps the single-crystallinity, the change in polarity caused by molecular motion may open up new dielectric properties. In this study, we introduced a supramolecular cation composed of DB18C6 and the branched-chain alkylammonium, isobutylammonium$^+$ (iBA$^+$), into the [Ni(dmit)$_2$]$^-$ salt. The resulting (iBA$^+$)(DB18C6)[Ni(dmit)$_2$]$^-$•0.4CH$_3$CN (**1**•0.4CH$_3$CN) maintained its single-crystal nature even though 60% of the CH$_3$CN sites were CH$_3$CN-free void, due to the dynamic behavior of iBA$^+$ cations adjacent to the void sites in crystal. Void sites are randomly arranged like Swiss cheese in the crystal. Polarization originating from the molecular motion of iBA$^+$ in Swiss cheese-like void domains showed relaxor-like dielectric anomalies.

Fig. 1 shows the structure of crystal **1**•0.4CH$_3$CN at 200 K. The crystal system and space group are monoclinic and $P2_1/m$, respectively (Table S1). In the crystal, one molecule each of iBA$^+$ and CH$_3$CN (occupancy about 0.4), and half structure each of DB18C6 and [Ni(dmit)$_2$]$^-$ are crystallographically independent (Fig. S1). As-grown crystals were stable up to 340 K and lost 1.9wt% before decomposition at 430 K by thermogravimetry analysis (Fig. S2). This weight corresponds to 0.4 molecules of CH$_3$CN (1.8wt%) per crystal composition. iBA$^+$ and DB18C6 formed N-H•••O hydrogen bonds to form supramolecular cations with a composition ratio of 1:1. The supramolecular cations and CH$_3$CN are stacked alternately along the *a* axis and arranged in a one-dimensional (1D) chain. The 1D chains aligned parallel to adjacent 1D chains in the ±*c* axis direction, forming a two-dimensional (2D) layer on a plane parallel to the *ac* plane (**Fig. 1a**). There are no molecular contacts between the supramolecular cations below the van der Waals (vdW) radius. The [Ni(dmit)$_2$]$^-$ is in close contact with the neighboring [Ni(dmit)$_2$]$^-$ in a side-by-side manner with the nearest sulfur interatomic distance of 3.380(2) Å, forming a 2D layer on a plane parallel to the *ac* plane. 2D layers composed of supramolecular cations and CH$_3$CN alternate with 2D layers composed of [Ni(dmit)$_2$]$^-$ along the *b* axis (**Fig. 1b**).

The structure of disorder sites in crystal **1**•0.4CH$_3$CN is summarized in **Fig. 2**. iBA$^+$ is disordered at four sites and two sites are crystallographically independent. The sites with iBA$^+$ occupancies of 0.396(9) and 0.104(9) at 200 K are denoted as **A** and **B**, respectively, and the sites crystallographically equivalent to **A** and **B** are **A′** and **B′**, respectively (**Fig. 2b**). As shown in **Fig. 2c**, the CH$_3$CN molecule is arranged across the crystallographic mirror plane, so that the composition of CH$_3$CN per crystal composition is about 0.4. The nearest-neighbor carbon•••carbon atomic distance between the CH$_3$CN and iBA$^+$ at the **B** or **B′** sites is 2.39(6) Å, indicating

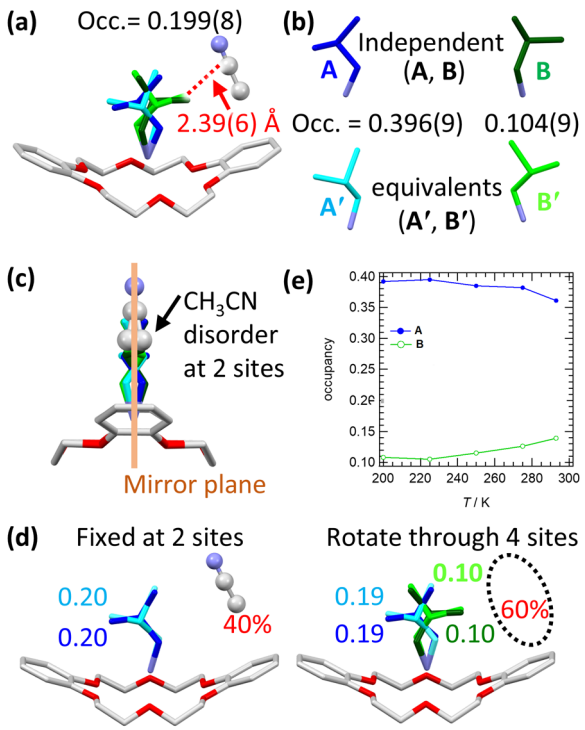

Fig. 2. Disorder sites in **1**•0.4CH_3CN at 200 K. (a) Structure of supramolecular cation and nearest CH_3CN. Red dotted line corresponds to the nearest C•••C distance between CH_3CN and **B** site of iBA^+. (b) Disordered sites of iBA^+ and their occupancy. (c) Supramolecular cation and the nearest CH_3CN viewed along the *c* axis. CH_3CN showed two-site disordering due to the mirror plane. (d) Structure of disordered sites with and without CH_3CN. Almost 40% of iBA^+ are fixed at **A** and **A'** sites due to the steric hindrance (left), while 60% of iBA^+ disordered through 4 sites (right). (e) Temperature dependence of occupancy for **A** and **B** sites of iBA^+.

that the CH_3CN and iBA^+ at the **B** and **B'** sites are approximately 1 Å closer than the sum of the vdW radii of the two carbon atoms, 3.4 Å (Fig. 2a). Therefore, due to steric hindrance between CH_3CN and **B**-site iBA^+, CH_3CN and the **B** and **B'** sites of iBA^+ cannot exist simultaneously. iBA^+ adjacent to CH_3CN is always at the **A** or **A'** site. In the crystal, about 40% of the CH_3CN-assigned sites are occupied, while 60% are voids. The **A** and **A'** occupancies of iBA^+ adjacent to CH_3CN are both about 0.2 (left in Fig. 2d). iBA^+ adjacent to 60% vacant sites can also take **B** and **B'** sites (right in Fig. 2d). The occupancy of the **B** site is 0.106(9) at 200 K. The occupancy of the **A** next to the vacant site can be regarded as about 0.2. In other words, 40% of the iBA^+ adjacent to CH_3CN is at the **A** site, and 40% of the 60% adjacent to the void site is at the **A** site. The remaining 20% is present at the **B** site to fill the missing hole of CH_3CN. Molecular crystals containing crystalline solvent usually have difficulty in maintaining single crystallinity due to the rearrangement of the molecules as the crystalline solvent is desorbed. In crystal **1**•0.4CH_3CN, despite the presence of 60% solvent-free defect sites, the single-crystalline nature is maintained because iBA^+ is disordered between the four sites and fills the space.

To evaluate the molecular volume occupied by disordered iBA^+, the size of voids was compared for model crystals with CH_3CN removed, when iBA^+ was present only at the **A** site and when iBA^+ was disordered at all sites. Voids were calculated using Mercury software in contact surface mode with 1.2 Å of probe radius and 0.1 Å of grid spacing. In the case where iBA^+ is present only at the **A** site of the crystal, the size of the void is 77.36 $Å^3$ per crystal composition, corresponding to 7.6% of the unit cell. In contrast, the model with iBA^+ disordered at four sites has 38.89 $Å^3$ of voids per crystal composition, which corresponds to 3.8% of the unit cell. Disordered iBA^+ occupies an extra space of about 40 $Å^3$, which plays an important role in stabilizing defect sites. The 38.89 $Å^3$ per crystal composition of the **1**•0.4CH_3CN crystal is within a reasonable range, given that several examples of molecular ionic crystals with voids of around 40-140 $Å^3$ per crystal composition have been reported.[16,17]

To evaluate the molecular motion of iBA^+, single-crystal X-ray structure analysis of **1**•0.4CH_3CN was performed every 25 K from 200-293 K. The results of the occupancy of the **A** and **B** sites are summarized in Fig. 2e. The occupancy of CH_3CN is almost independent of temperature, with negligible desorption of CH_3CN from the crystals on the time scale of X-ray diffraction measurements in the temperature range up to 293 K (Fig. S3). The occupancy of the **A** and **B** sites was almost constant below 225 K, but the occupancy of the **B** site gradually increased above 225 K, reaching 0.139(5) at 293 K. Occupancy changes with increasing temperature above 225 K suggests that iBA^+ is in motion at least above 225 K.

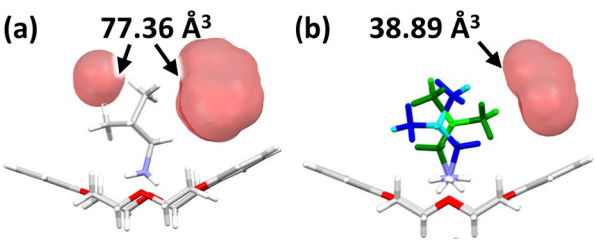

Fig. 3. Void space in model crystals with CH_3CN removed. (a) Supramolecular cation model with ordered iBA^+. Void space is 77.36 $Å^3$ / formula. (b) In the model with disordered iBA^+ at four positions, the space is 38.89 $Å^3$/ formula.

The molecular motion was also supported by temperature-dependent measurements of dielectric constant (**Fig. S4**). The real part of the dielectric constant (ε_1) sharply increased from around 230 K, which correspond to the temperature dependence of iBA^+ occupancy. This result indicates that the molecules in the crystal are in motion above this temperature. It should be noted that ε_1 has peaks around 270 K, unlike the usual Debye-type relaxation. These peaks strongly suggest a relaxor-like dielectric behavior originating from nanometer-sized polarized domains within the crystal.[11,18,19] Since the voids in the crystal are randomly distributed, Swiss cheese-like void domains should exist in the crystal. If the iBA^+ cations in the domains move cooperatively, nano-sized polarized domains should form.

The temperature dependence of the molar magnetic susceptibility (χ_m) of **1**•0.4CH_3CN under a static magnetic field of 1 T was measured in the range from 1.8 K to 300 K (**Fig. 4**). The decrease in the value of $\chi_m T$ with decreasing temperature at low temperatures suggests the antiferromagnetic interactions between $[Ni(dmit)_2]^-$. Indeed, the temperature dependence of $\chi_m T$ followed the Curie-Weiss law with a Curie constant of 0.392(1) cm^3 K mol^{-1} and a Weiss temperature of −4.96(9) K.

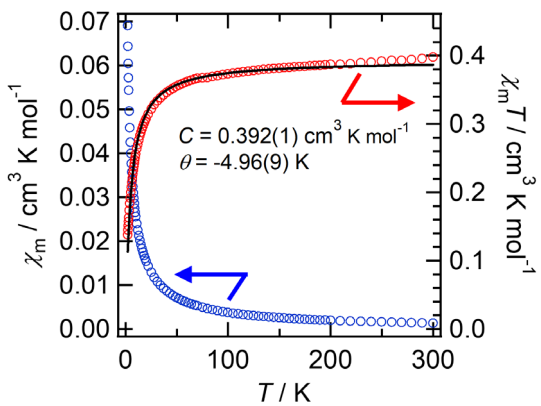

Fig. 4. Temperature dependence of the molar magnetic susceptibility of **1**•0.4CH_3CN, Blue and red circles and black line correspond to the experimental χ_m and $\chi_m T$ values and the best fitting described in the text. *C* and θ are the Curie constant and the Weiss temperature for fitting, respectively.

A supramolecular cation consisting of the branched-chain alkylammonium isobutylammonium$^+$ (iBA^+) and dibenzo[18]crown-6 was introduced into $[Ni(dmit)_2]^-$ salt, and (iBA^+)(dibenzo[18]crown-6)$[Ni(dmit)_2]^-$•0.4CH_3CN (**1**•0.4CH_3CN) was prepared. In crystal, 60% of the sites occupied by CH_3CN are voids; iBA^+ with molecular motion occupies about 40 $Å^3$ extra space per crystal composition compared to that without molecular motion, thus preserving single-crystal nature. In most molecular crystals, void sites created by solvent desorption are the main cause of crystalline collapse. In crystal **1**•0.4CH_3CN, not only was the structure maintained by the motion of iBA^+ cations adjacent to the voids, but also the polarization was reversed as a result of molecular motion. Furthermore, randomly distributed voids within the crystal formed Swiss cheese-like domains, and the cooperative motion of the iBA^+ cations formed polarized nanodomains that exhibited a relaxor-like dielectric response. The active use of molecular motion in crystals with random voids provides a new perspective for the design of molecular dielectrics that exhibit relaxor responses.

Acknowledgement

The authors thank Dr. Shuhei Fukuoka and Prof. Satoaki Matsunaga of the Faculty of Science, Hokkaido University, for χ_m measurements.

Supplementary data

Supplementary material is available at *Chemistry Letters.*

Funding

This study was financially supported by JSPS KAKENHI (grant no. JP22H00311), JST ACT-X (grant no. JPMJAX23DB), the research project of "Crossover Alliance to Create the Future with People, Intelligence and Materials", and Research Program of "Network Joint Research Center for Materials and Devices", from the Ministry of Education, Culture, Sports, Science and Technology of Japan (MEXT).

Conflict of interest statement. None declared.

References

1 A. I. Kitaigorodskii, *Acta Cryst* **1965**, *18*, 585.
2 Y. Yakiyama, T. Fujinaka, M. Nishimura, R. Seki, H. Sakurai, *Chemical Communications* **2020**, *56*, 9687.
3 M. Mastalerz, *Chemistry – A European Journal* **2012**, *18*, 10082.
4 H. Yamagishi, H. Sato, A. Hori, Y. Sato, R. Matsuda, K. Kato, T. Aida, *Science* **2018**, *361*, 1242.
5 S. J. Dalgarno, P. K. Thallapally, L. J. Barbour, J. L. Atwood, *Chem. Soc. Rev.* **2007**, *36*, 236.
6 A. Be¯rziņš, A. Trimdale, A. Kons, D. Zvaniņa, *Crystal Growth & Design* **2017**, *17*, 5712.
7 J. E. Clements, P. R. Airey, F. Ragon, V. Shang, C. J. Kepert, S. M. Neville, *Inorg. Chem.* **2018**, *57*, 14930.
8 N. Hoshino, T. Akutagawa, *Crystal Growth & Design* **2021**, *21*, 4640.
9 F. Kobayashi, Y. Komatsumaru, R. Akiyoshi, M. Nakamura, Y. Zhang, L. F. Lindoy, S. Hayami, *Inorg. Chem.* **2020**, *59*, 16843.
10 A. I. Kitaigorodsky, *Mixed crystals*, Springer Science & Business Media, **2012**.

11 S. Li, K. Takahashi, R. K. Huang, C. Xue, K. Kokado, N. Hoshino, T. Akutagawa, S. Nishihara, T. Nakamura, *Chemistry of Materials* **2023**, *35*, 2421.
12 K. Takahashi, Y. Shirakawa, H. Sakai, I. Hisaki, S. I. Noro, T. Akutagawa, M. Nakano, T. Nakamura, *Journal of Materials Chemistry C* **2023**, *11*, 1891.
13 K. Takahashi, T. Nakamura, T. Akutagawa, *Coordination Chemistry Reviews* **2023**, *475*, 214881.
14 T. Akutagawa, K. Shitagami, S. Nishihara, S. Takeda, T. Hasegawa, T. Nakamura, Y. Hosokoshi, K. Inoue, S. Ikeuchi, Y. Miyazaki, K. Saito, *Journal of the American Chemical Society* **2005**, *127*, 4397.
15 T. Akutagawa, H. Koshinaka, D. Sato, S. Takeda, S.-I. Noro, H. Takahashi, R. Kumai, Y. Tokura, T. Nakamura, *Nature Materials* **2009**, *8*, 342.
16 J. S. Costa, S. Rodríguez-Jiménez, G. A. Craig, B. Barth, C. M. Beavers, S. J. Teat, G. Aromí, *J. Am. Chem. Soc.* **2014**, *136*, 3869.
17 M. Fujibayashi, Y. Watari, R. Tsunashima, S. Nishihara, S. Noro, C.-G. Lin, Y.-F. Song, K. Takahashi, T. Nakamura, T. Akutagawa, *Angewandte Chemie International Edition* **2020**, *59*, 22446.
18 S. Horiuchi, R. Kumai, Y. Okimoto, Y. Tokura, *Chemical Physics* **2006**, *325*, 78.
19 L.-L. Zhang, Y.-N. Huang, *Sci Rep* **2020**, *10*, 5060.

Supporting Information for

Molecular Motion in Supramolecular Ionic Crystal of Swiss Cheese Structure

Kazuya Kanamaru,[1] Kiyonori Takahashi,[1,2*] Rui-Kang Huang,[1,2] Chen Xue,[1,2] Jia-bing Wu,[1,2] Shin-ichiro Noro[3] and Takayoshi Nakamura[1,2,4*]

E-mail: ktakahashi@es.hokudai.ac.jp (K. Takahashi), tnaka@es.hokudai.ac.jp (T. Nakamura)

Contents

§1. Experimental Section

Synthesis

All reagents purchased were used without further purification. Precursor of $(TBA^+)[Ni(dmit)_2]^-$ (TBA^+= tetra-*n*-butylammonium$^+$) was prepared using a procedure reported in the literature.[S1] A solution of $(TBA^+)[Ni(dmit)_2]^-$ (40 mg, 0.0576 mmol) in CH_3CN (10 mL) was added to a solution of dibenzo[18]crown-6 (350 mg, 0.97 mmol) and isobutylammoium chloride (66 mg, 0.0602 mmol) in the mixture of CH_3OH (2 mL) and CH_3CN (20 mL). Crystal **1**•0.4CH_3CN was obtained by slow diffusion over a period of 7-14 days.

Crystal structure determination

Temperature-dependent structural analysis of the single crystal **1**•0.4CH_3CN was performed using a Rigaku XtaLAB-Synergy diffractometer with a HyPix-6000 area detector and multilayer mirror-monochromated Mo Kα radiation (λ = 0.71073 Å). A single crystal was mounted on a MicroMountsTM tip (MiTeGen) with Paratone 8277 (Hampton Research). For the reflection data, multi-scan absorption corrections were applied to the crystal. Data collection was performed and processed using the CrysAlisPRO interface (Oxford Diffraction, Agilent Technologies UK Ltd). The initial structure was solved using SHELXT,[S2] and structural refinement was performed using

OLEX2 software.[S3] Anisotropic refinement was applied to all atoms, except for the hydrogen atoms. Crystallographic data was deposited at Cambridge Structural Database Center with CCDC deposition numbers 2392008, 2392009, 2392010, 2392011, and 2392012 for crystal **1**•0.4CH_3CN at 200, 225, 250, 270, and 293 K, respectively.

Magnetic Properties

The temperature-dependent magnetic susceptibility for a polycrystalline sample of **1**•0.4CH_3CN was measured using a Quantum Design MPMS-3 SQUID magnetometer. Prior to sample measurement, the magnetic susceptibility of the sample holder (aluminum foil) was measured under identical conditions, then the susceptibility of the holder was subtracted from the gram susceptibility as the paramagnetic contribution. The diamagnetic contribution of the diamagnetic component in the sample was subtracted based on Pascals constant, -5.124×10^{-4} cm^3 mol^{-1}.[S4] A magnetic field of 1 T was applied for all temperature-dependent measurements. Molecular weight of 902.3 g mol^{-1} (the molar susceptibility for one $[Ni(dmit)_2]^-$ molecule) was used for calculation of the molar magnetic susceptibility of crystal **1**•0.4CH_3CN.

Thermal Analysis

Thermogravimetric-differential thermal analysis (TG-DTA) was conducted using a *Rigaku* Thermo Plus TG8120 with 10 K/min heating rate under nitrogen gas flow.

Dielectric Measurements

Temperature- and frequency-dependent dielectric constants were measured using an impedance analyzer 4294A (Agilent) using the four-probe AC impedance method at a frequency range of 10^2–10^5 Hz. The temperature was controlled using cryostats with temperature controller models 331 (Lake Shore Cryotronics Inc.). Electrical contacts were prepared using a gold paste to attach the 25 μm ϕ gold wires to the pelletized sample.

§2. Crystallographic Data

Table S1. Crystal data, data collection, and reduction parameters for crystal **1**•0.4CH_3CN.

Crystal	**1**•0.4CH_3CN		
Temperature / K	200	225	250
Chemical formula, Formula Weight	$C_{30.80}$ $H_{37.19}$ $N_{1.40}$ Ni O_6 S_{10}, 902.26		
Crystal system, space group	Monoclinic, $P2_1/m$		
a, Å	8.5981(7)	8.6152(2)	8.6462(3)
b, Å	20.4774(17)	20.5252(6)	20.5807(8)
c, Å	11.5423(8)	11.5562(3)	11.5555(4)
α, deg	90	90	90
β, deg	93.495(7)	93.698(2)	93.522(3)
γ, deg	90	90	90
V, Å^3	2028.4(3)	2039.21(9)	2052.36(13)
Z	2		
D_{calc}, g·cm^{-3}	1.477	1.469	1.459
μ,(Mo K_α) cm^{-1}	1.034	1.029	1.022
$2\theta_{max}$, deg	58.094	59.594	62.324
Reflections measured	17853	23152	42521
Independent reflections	4279	4301	42521
Reflections used	4279	4301	42521
R_1[a]	0.0614	0.0460	0.0639
$R_w(F^2)$[b]	0.1710	0.1263	0.1926
GOF	1.126	1.169	1.119
CCDC No.	2392008	2392009	2392010

Crystal	**1**•0.4CH_3CN	
Temperature / K	275	293
Chemical formula, Formula Weight	$C_{30.80}$ $H_{37.19}$ $N_{1.40}$ Ni O_6 S_{10}, 902.26	
Crystal system, space group	*Monoclinic, P*2_1*/m*	
a, Å	8.6595(3)	8.6787(3)
b, Å	20.5863(7)	20.6346(6)
c, Å	11.5513(3)	11.5615(3)
α, deg	90	90
β, deg	93.707(3)	93.755(3)
γ, deg	90	90
V, Å^3	2054.91(11)	2066.01(11)
Z	2	
D_{calc}, g·cm^{-3}	1.458	1.449
μ,(Mo K_α) cm^{-1}	1.021	1.015
$2\theta_{max}$, deg	58.366	56.23
Reflections measured	23363	37571
Independent reflections	4332	4352
Reflections used	4332	4352
R_1[a]	0.0474	0.0355
$R_w(F^2)$[b]	0.1285	0.0994
GOF	1.162	1.033
CCDC No.	2392011	2392012

[a] $R_1 = \sum||F_o| - |F_c|| / \sum|F_o|$ and [b] $R_w = (\sum\omega(|F_o| - |F_c|)^2 / \sum\omega F_o^2)^{1/2}$.

§3. Crystallographically independent structure

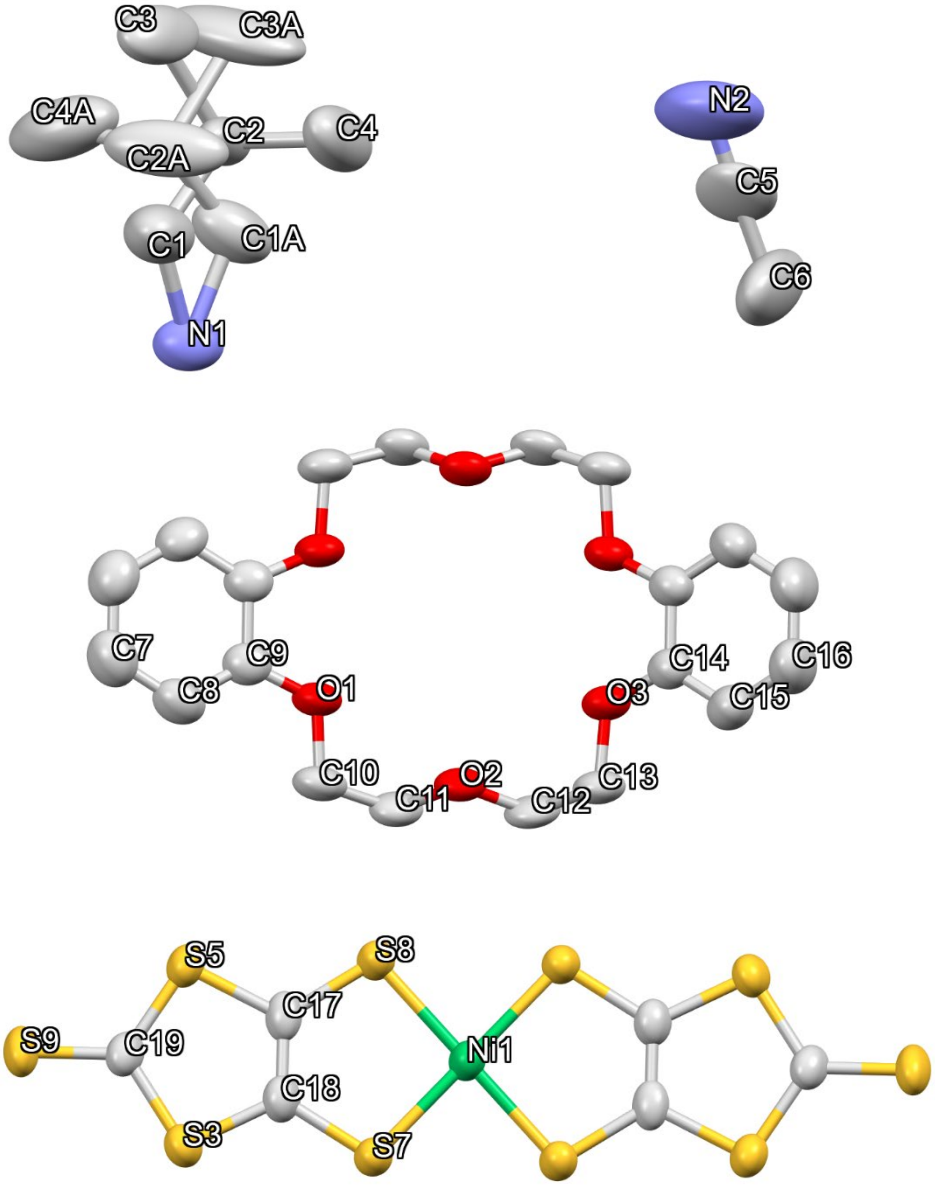

Fig. S1. Molecular structures in **1**•0.4CH_3CN with thermal ellipsoid model with 50% probability. Labeled atoms are crystallographically independent. Hydrogen atoms are omitted for clarity.

§4. Thermal Stability

To evaluate the thermal stability, thermogravimetry analysis was applied to the polycrystalline sample of **1**•0.4CH_3CN and summarized in **Fig. S2**.

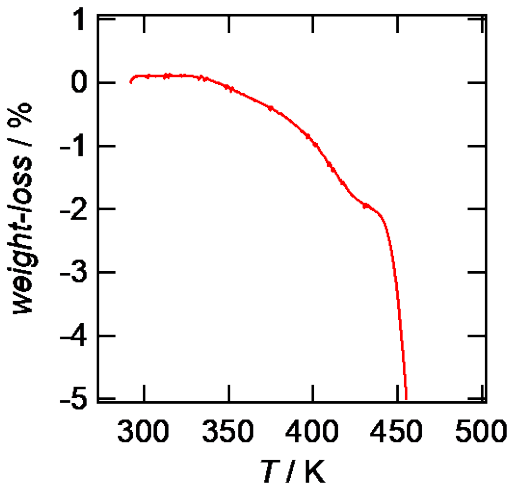

Fig. S2. Thermogravimetry of **1**•0.4CH_3CN.

Crystal **1**•0.4CH_3CN was thermally stable below 340 K. Weight loss was observed above 340 K, reached to 1.9 wt% at 430 K, and decomposed above 430 K. Weight loss of 1.9 wt% correspond to the desorption of 0.4 molecules of CH_3CN per crystal composition of **1**•0.4CH_3CN.

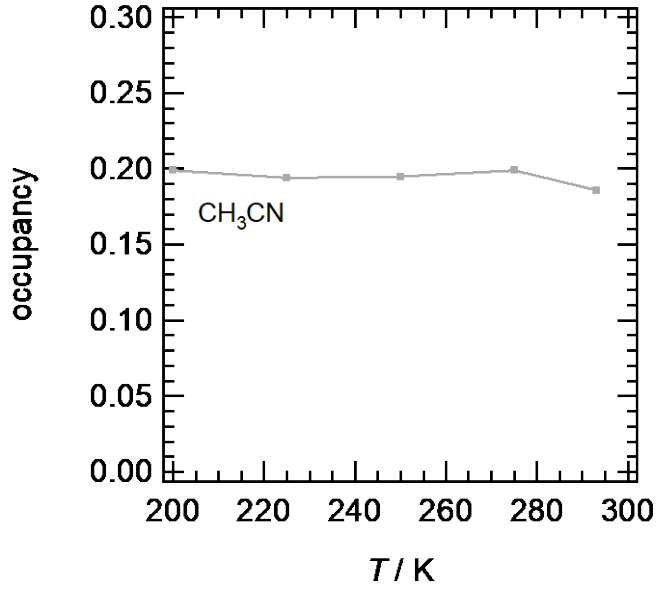

Fig. S3. Temperature dependence of occupancy of CH_3CN in crystal **1**•0.4CH_3CN.

§5. Dielectric Property

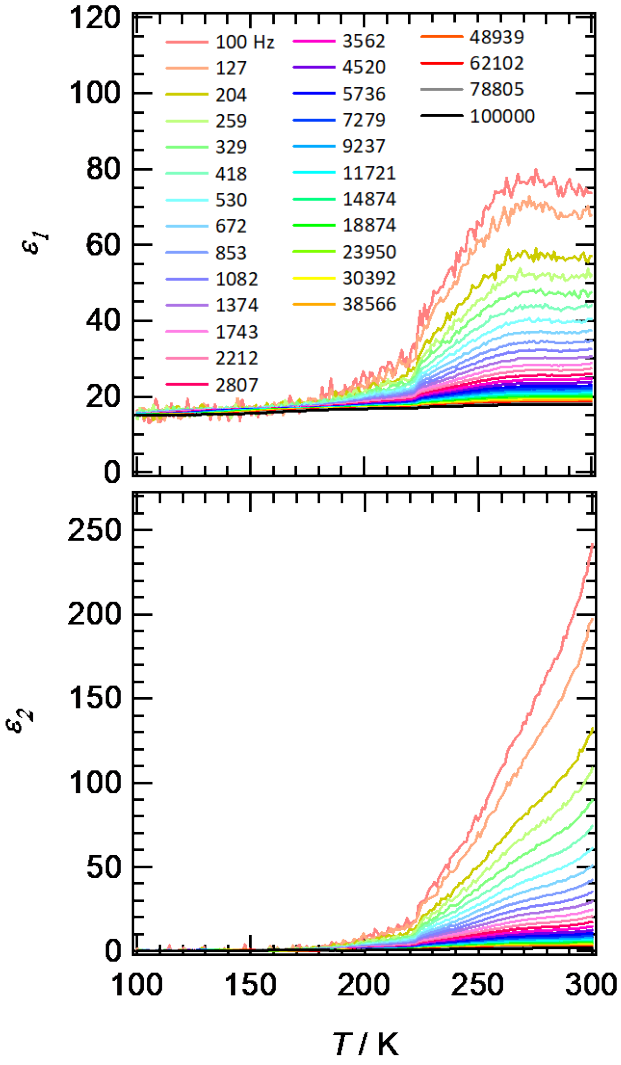

Fig. S4. Temperature- and frequency-dependent real and imaginary part of dielectric permittivity (ε_1 and ε_2, respectively) of pelletized sample of **1**•0.4CH_3CN.

§6. Reference

S1 G. Steimecke, H.-J. Sieler, R. Kirmse, E. Hoyer, *Phosphorous and Sulfur and the*

Related Elements **1979**, *7*, 49.

S2 G. M. Sheldrick, *Acta Crystallographica Section A Foundations and Advances* **2015**, *71*, 3.

S3 O. V. Dolomanov, L. J. Bourhis, R. J. Gildea, J. A. K. Howard, H. Puschmann, *Journal of Applied Crystallography* **2009**, *42*, 339.

S4 G. A. Bain, J. F. Berry, *Journal of Chemical Education* **2008**, *85*, 532.